Current Density Dependent Electroplating in Ca Electrolytes: From Globules to Dendrites

Shengda D. Pu[1†], Chen Gong[1†], Xiangwen Gao[1], Ziyang Ning[1], Sixie Yang[1], John-Joseph Marie[1,2], Boyang Liu[1,2], Robert A. House[1,2], Gareth O. Hartley[1,2], Jun Luo[3], Peter G. Bruce[1,2,4,5], Alex W. Robertson[1*]*

[1] Department of Materials, University of Oxford, Parks Road, Oxford OX1 3PH, United Kingdom
[2] The Faraday Institution, Quad One, Becquerel Avenue, Harwell Campus, Didcot, OX11 0RA, United Kingdom
[3] Center for Electron Microscopy and Tianjin Key Lab of Advanced Functional Porous Materials, Institute for New Energy Materials, School of Materials, Tianjin University of Technology, Tianjin, 300384, China
[4] Department of Chemistry, University of Oxford, South Parks Road, Oxford OX1 3QZ, United Kingdom
[5] The Henry Royce Institute, Parks Road, Oxford, OX1 3PH, United Kingdom
[†] These authors contributed equally to the manuscript.
* alex.w.robertson@gmail.com peter.bruce@materials.ox.ac.uk

Abstract

Multivalent cation rechargeable batteries, including those based on Ca, Mg, Al, etc., have attracted considerable interest as candidates for beyond Li-ion. Recent developments have realized promising electrolyte compositions for rechargeable Ca batteries; however, an in-depth understanding of the Ca plating and stripping behavior, and the mechanisms by which adverse dendritic growth may occur, remains underdeveloped. In this work, via in-situ transmission electron microscopy, we have captured the real-time nucleation, growth, and dissolution of Ca, the formation of dead Ca, and demonstrated the critical role of current density and the solid-electrolyte interphase layer in controlling the plating morphology. In particular, the interface was found to influence Ca deposition morphology, and can lead

to Ca dendrite growth under unexpected conditions. These observations allow us to propose a model explaining the preferred conditions for reversible and efficient Ca plating.

Multivalent cation batteries based on Mg, Ca, Al, etc. have attracted significant interest as potential candidates to replace Li-ion batteries in recent years.[1–5] These metallic anodes have much higher natural metal abundancy, and are reported to be much less prone to dendrite formation compared with metallic Li anode,[3–11] potentially due to their lower self-diffusion barriers.[1,12,13] The Ca-ion system has demonstrated significant potential. It has a comparable volumetric capacity to Li, and compared with other multivalent systems like Mg, it also has the advantages of higher earth abundance, lower reductive potential and lower charge density.[1] Despite this, the development of Ca-ion batteries has been slow in part due to issues with the anode, where most studied electrolytes react with metallic Ca, rapidly forming surface passivation layers comprised of $CaCl_2$, $Ca(OH)_2$, or $CaCO_3$, that block Ca ion diffusion and make further plating impossible.[14–17] However, recent breakthroughs in electrolyte research have brought renewed interest in Ca-ion batteries.[18–21] These works have demonstrated promising Ca-based electrolytes that are capable of continuous plating and stripping with relatively high efficiency at moderately elevated[17] or room-temperatures.[4,11,22] While most previous studies demonstrated fairly smooth plating morphology,[3–11] a recent paper by Davidson *et al*.[23] showed that dendrites do grow in Mg-ion electrolyte. This challenges the widely accepted belief that multivalent systems do not form dendrites easily. Since research into Ca-ion electrolytes is at an early stage, little work has been done to systematically study their plating and stripping processes. This study explores the electroplating morphology and mechanism within the Ca-ion system via in situ transmission electron microscopy (TEM) to evaluate the feasibility of employing metallic Ca anodes, and to provide a deeper understanding of this system for future optimization.

The electrolyte used in this work is 1 M $Ca(BH_4)_2$ in tetrahydrofuran (THF), as per Wang *et al.*[4] (see methods). Cyclic voltammetry was used to evaluate the electrolyte in a 3-electrode cell, showing high coulombic efficiency (Supporting Figure S1). To explore the relationship between the plating morphology and current density, Ca plating at various current densities were studied with in-situ liquid cell TEM. The liquid cells were constructed as depicted in Supporting Figure S2, where Pt was used for the working, counter and reference electrodes. TEM imaging was performed at a low electron dose rate of ≤ 0.04 electrons $Å^{-2}$ s^{-1}, to minimize any beam effect.[24] The driven current density is calculated as the total current applied by the potentiostat, divided by the exposed Pt electrode surface area measured with scanning electron microscope (SEM) images. Due to the small size of the electrode this current density could be exaggerated, and the real current density could be smaller due to any electrode roughness and porosity increasing its effective area.

The plating morphology was first studied at a 100 mA cm^{-2} current density, revealing the formation of dendrites. Four galvanostatic cycles were performed. For each cycle, a negative bias was applied for 15 seconds, followed by a positive bias for another 15 seconds. The load curve of the first two cycles together with the relevant TEM images are shown in Figure 1a and Figure 1b, with all four cycles shown in Supporting Movie S1. From Figure 1a i and ii, it can be seen that as soon as the negative potential was applied, a sharp dendrite nucleated from the tip of the Pt electrode and rapidly grew out of the field of view within less than a second. This dendritic growth has not been reported in Ca-ion systems,[4,10] but is similar to previous studies in Li-ion systems with a similar cell setup.[24,25] Upon reversing the current, some Ca dendrites gradually detached from the Pt electrode and drifted away, as indicated by the white arrows in Figure 1a iii and iv, which can be seen more clearly in Supporting Movie S1. This corresponds to the stripping process and formation of 'dead calcium'.[4] Just like the 'dead lithium' observed in Li-ion batteries,[26] these 'dead calcium' are electrically isolated from the electrode, resulting in inactive Ca

deposits that cannot be stripped away, and thus reduced coulombic efficiency. Also of interest are the features denoted with black arrows at 17 and 26 seconds in Figure 1a v, which are indicative of short-circuit events. This suggests that the two Pt electrodes, 200 microns apart, had been bridged by the deposited Ca metal within 17 seconds, suggesting a rapid dendrite growth rate of at least 11.7 μm s^{-1}.

In the second cycle (Figure 1b), sharp dendrites nucleated from the gaps unoccupied by the existing Ca dendrites, as indicated by the yellow arrows in Figure 1b i. After dendrite formation was initiated and upon further Ca deposition, the initially sharp dendrite tips expanded into a globular structure (magnified and annotated images Figure 1b vi-xi). This 'dendrite tip blunting' phenomenon was observed in all four cycles and will be discussed later. Upon reversing the current, Ca stripping was observed, indicated by the red circles in Figure 1b ii and iii, as a Ca deposit gradually reduced in size and finally disappeared. With continued application of the reversed bias, more dendrites formed on top of the existing Ca deposits, originating from outside the field of view away from the working electrode, causing another short-circuit (black arrow, Figure 1b v). This suggests that these dendrites were from plating on the counter electrode, and grew across to the working electrode (Supporting Movie S1). As more dendrites formed, such short-circuit events became more frequent, demonstrated in the 3rd and 4th cycles (Supporting Figure S3a and S3b).

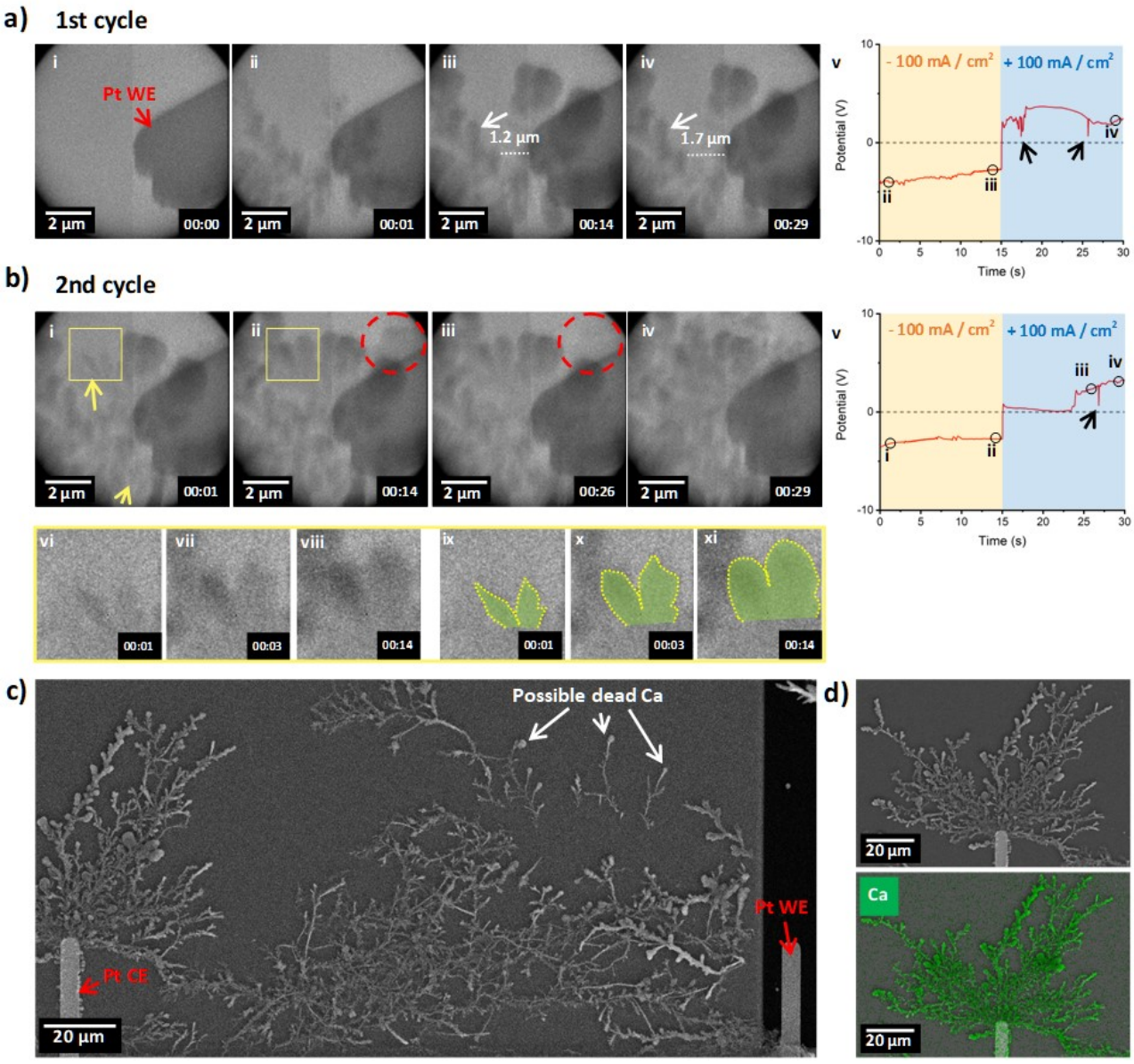

Figure 1. Dendritic growth from Ca electrolyte under high current density. In-situ electrochemical TEM of (a) the first galvanostatic cycle and (b) the second galvanostatic cycle (Supporting Movie S1). (c) SEM image of the disassembled cell after an in-situ TEM experiment, showing the short circuiting between the two electrodes from Ca dendritic growth. (d) SEM and EDS mapping of the counter electrode.

After four cycles, the liquid-cell was purged by flowing tetrahydrofuran (THF), disassembled in an argon glovebox, and the post-mortem Ca deposit examined under SEM *via* an environmental transfer unit, screening it from air exposure (Figure 1d). From Figure 1d, it is clear that the deposited dendrites

have bridged between the working and counter Pt electrodes, which further confirmed the origin of the short-circuit events. (Note: most of the Ca deposit on the working electrode was unavoidably lost during cell disassembly). In addition, some Ca dendrites were detached from the rest of the deposit and the electrodes, as indicated by the white arrows. These are likely to be 'dead calcium' dendrites, as per our previous observation under TEM in Figure 1a iii and iv, that stuck to the cell window. The dendrites formed at the Pt counter electrode were characterized by energy-dispersive x-ray spectroscopy (EDS) mapping, confirming these dendrites to consist of Ca (Figure 1e). Higher magnification SEM images of the dendrites' morphology are shown in Supporting Figure S4, which reveal the characteristic branching fractal structure, comparable to those reported in other metallic systems.[27–29]

We performed further in-situ TEM studies at lower 1 mA cm^{-2} and 10 mA cm^{-2} current densities, to explore the plating morphology at more representative current densities for a practical cell. The results are summarized in Figure 2a and b, with the full sequences in Supporting Movies S2 and S3. The corresponding charging curves are shown in Supporting Figures S5 and S6. Unlike in the 100 mA cm^{-2} case, gradual globular growth occurs with a more uniform coverage of the Pt electrode when plating at 1 mA cm^{-2}, with no dendrite formation observed. When an intermediate current density of 10 mA cm^{-2} was applied, the electroplated Ca still exhibited globular growth with larger size than that in the 1 mA cm^{-2} case, with no clear dendrites observed. These observations show that plating morphology is dependent on current density, and explain the 'dendrite tip blunting' phenomenon observed during plating at 100 mA cm^{-2}: Dendrite formation substantially increased the overall plating surface area and changed the current distribution, effectively lowering the local current density at certain plating sites, leading to a dendrite-to-globule transition with further Ca deposition at sites where the local current density reduced over time with plating.

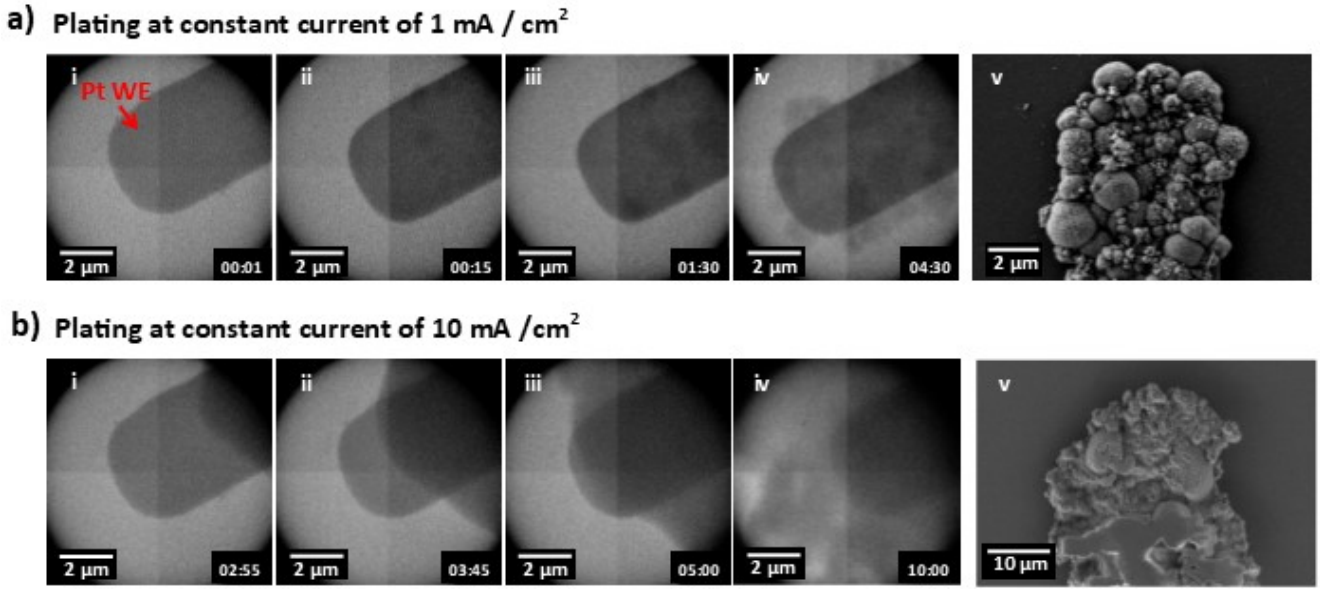

Figure 2. Globular Ca plating at lower current densities. Ca plating at (a) -1 mA cm^{-2} and (b) -10 mA cm^{-2}. Panels i-iv show the in-situ electrochemical TEM recording, panel v show SEM images of the electrode after disassembling the liquid-cell.

To construct a comprehensive understanding of this current-density dependent morphology transition, several in-situ TEM cells plated with the same capacity at different current densities were disassembled and their post-mortem deposits were studied under SEM. A transition from globular/island to dendritic growth was seen as the plating current density was increased from 10 to 20, 50 and 100 mA cm^{-2} (Figure 3a i-iv). Each study passed 18 µC total charge, with different amounts of Ca deposition imaged due to losses during cell disassembly. This current density dependent transition from globular/island to dendritic growth is consistent with the conventional model used to describe electrodeposition growth (Figure 3b), and is also consistent with the previous theory proposed for Li-ion battery systems. At higher current densities, the ion diffusion rate towards the plating interface is not fast enough to compensate the ion depletion rate due to reduction and deposition, with this loss of equilibrium leading to dendrite formation.[30]

Based on this morphology-current relation, a critical current density limit for ion depletion, and thus dendrite formation, can be roughly estimated for our in-situ TEM electrochemical cell. With a flow rate of 80 μL hr^{-1}, it takes less than a second to replace all the electrolyte within the enclosed cell, which allows the ion concentration to be restored to the nominal value of 1 M. Using the diffusion length equation $d = \sqrt[2]{4 \cdot D_{\mathrm{Ca}} \cdot t}$ (d is the diffusion length, t is the time allowed for diffusion, D_{Ca} is the Ca ion diffusion coefficient, which is estimated to be 7.4×10^{-7} cm^2 s^{-1} for this system by Kim, *et al.*[10]), we can estimate the limiting Ca deposition rate at the surface to be 1.7×10^{-6} mol cm^{-2} s^{-1}, which corresponds to a limiting plating current density of 55 mA cm^{-2}. (Note: We took into account that the current density at the edge of the electrode is three times higher than the nominal applied current density.[23]) This value is comparable to some of the reported values in Li-ion battery systems.[30,31] It should be noted that this value is estimated specifically for our system (1 M $Ca(BH_4)_2$ in THF within the electrochemical liquid-cell TEM set-up) and cannot necessarily be directly applied to other systems. The critical current density is expected to be lower for most other systems, as there is no constant electrolyte replenishment, and the overall applied current is larger due to their bigger electrode size. Even within our system, this value is somewhat overestimated since we do see evidence of dendrite formation at 50 mA cm^{-2}, as shown in Figure 3b iii. This is most likely because the diffusion of the Ca ions is limited within the confined sub-micron space between the encapsulating cell membranes, a phenomenon that has been previous reported in liquid-cell TEM set-ups.[32–35]

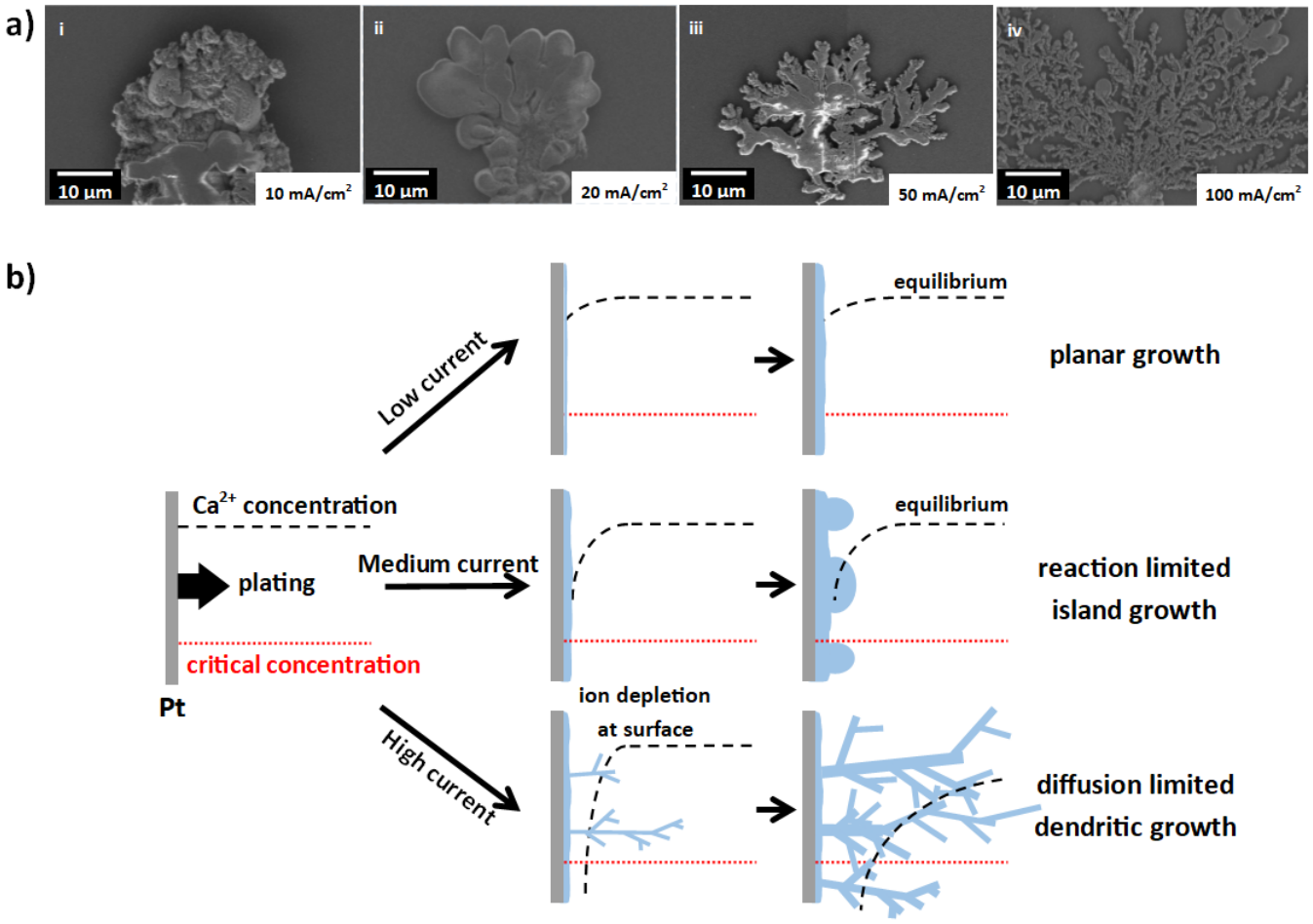

Figure 3. Current-density dependent plating morphology transition. (a) i-iv: SEM images of the Ca plating morphology for 10m 20, 50, and 100 mA cm^{-2}, showing a change from globular to dendritic deposition with increased current density. (b) Illustration showing a model for expected electrodeposition growth.

Our presented in-situ TEM studies are consistent with the expected model for the current density dependence of electroplating morphology, however deviations from it were observed. Figure 4a i shows the morphology of a further Ca deposit plated under the same conditions as the 10 mA cm^{-2} deposition in Figure 3a. Despite the overall globular morphology being consistent with our previous results, upon closer examination of the region highlighted by the red box dendrite formation can be seen (Figure 4a ii). This is unexpected at such a relatively low current density according to the standard electroplating model discussed earlier, and which is even lower than the typically reported current density for dendrite

formation in Li-ion systems.[30,31] This observation suggests an additional factor governing the conditions for dendrite growth when cycling a Ca electrolyte. We propose that the presence of an irregular solid electrolyte interface (SEI) layer explains our observations. The irregularity of this SEI leads to the presence of local current density inhomogeneities during plating,[4,10] and thus yields local high-current concentration spots. These 'hot spots' could exhibit current densities significantly higher than the nominal current density, and so dendrites could potentially nucleate from these spots. In addition, variations in the geometry of the plated deposit will assist dendrite growth, with hollows and recesses such as those visible in Figure 4a i potentially causing localized electrolyte depletion.

Post-mortem cross-sectional SEM imaging of a Au foil working electrode from an electrolytic cell, potentiostatically plated at -1 V vs. Ca for 5 hrs (corresponding to a current density of 5 to 10 mA cm^{-2}), reveals similar localized dendrite formation at low current densities (Figure 4b, Supporting Figure S7). This phenomenon is illustrated schematically in Figure 4d. We suggest that this 'hot-spot' dendrite formation can result in failures in standard Ca cells; we observe heavy and irregular Ca plating in an electrolytic cell operated under relevant current densities (Figure 4c), using a Pt foil working electrode with 1 cm^2 surface area and a Ca counter electrode with galvanostatic plating at 5 mA cm^{-2}. Dendrite-like Ca deposits can be seen, concentrating at the Pt foil edge. This indicates that dendrite formation is not necessarily a consequence of plating within a confined nanoscale space at high current density, but can also occur in macroscopic spaces under relatively low current density.

X-ray diffraction (XRD) was employed to explore the existence of any crystallized species in the SEI, using a conventional two-electrode cell cycled at 1 mA cm^{-2} for 10 hours with metallic Ca plates as both electrodes, each with a surface area of around 20 mm^2. Additional peaks appeared on the working electrode after cycling (blue line), Figure 4e, corresponding to the formation of CaH_2, whose reference XRD pattern is shown for comparison. The formation of the additional chemical component on the foil

after cycling is likely attributable to the formation of a CaH_2 containing SEI layer, suggested by previous studies with this electrolyte,[4] however it is likely that it is accompanied by additional organic components.

To better understand CaH_2 formation in the SEI and its relationship with current density and capacity, differential electrochemical mass spectrometry (DEMS) was used to quantify the plating at different conditions as shown in Figure 4f-h (see Methods). Figure 4e shows that, when plated at 0.2 mA cm^{-2}, the CaH_2/Ca ratio declined with increasing deposition time and stabilized at around 10%. This suggests that most of the CaH_2 formed at the beginning of the plating with fresh Ca deposits, and that the presence of CaH_2 prevented the newly deposited Ca from undergoing further side reactions with the electrolyte. A similar trend was observed at 1 mA cm^{-2} during plating, as shown in Figure 4f, with 70.9 % of Ca deposited in 20 mins and 86.2 % deposited in 100 mins. The relatively high CaH_2 content compared to previous work could be due to the lower electrolyte concentration and therefore less dissociation of $Ca(BH4)_2$ used in this work, suggesting the effect of electrolyte concentration in determining the cell performance. Figure 4g also shows that, when a reversed current was supplied to strip the plated deposit, the majority of the CaH_2 content remained while most of the Ca content disappeared. The remaining metallic Ca content after stripping is likely the 'dead calcium' electrically isolated from the electrode, consistent with our previous TEM observations. This also suggests that the CaH_2 SEI does not inhibit the stripping process of the metallic Ca, unlike passivating SEI layers previously reported in other Ca-ion systems.[14–17] We further increased the current density and compared the plating process under different current densities while keeping the total passed charge the same; i.e., plating at 0.2 mA cm^{-2} for 500 minutes, 1 mA cm^{-2} for 100 minutes and 5 mA cm^{-2} for 20 minutes. This is shown in Figure 4h. Similar amounts of CaH_2 were found at relatively low current densities, while a clear increase of the CaH_2 content from 10.2 % to 36.9 % was observed at 5 mA cm^{-2}. This could be due to the higher

overpotential applied for plating at 5 mA cm^{-2}, which could lead to the faster decomposition of THF that in turn may accelerate the formation of CaH_2, as suggested in ref. [4].

The formation of CaH_2 and the SEI has benefits and drawbacks. The presence of an SEI stops further reactions between the deposited Ca and the electrolyte, allowing extended plating at room temperature. However, despite not completely inhibiting the plating or stripping processes, the formation of the SEI led to slowing/partial blocking of Ca ion transport, which caused local current density inhomogeneity and unexpected dendrite growth. Therefore, it is important to consider the role of the SEI in Ca deposition, and its influence in instigating dendritic growth, when studying and developing Ca-ion electrolytes, which has been somewhat overlooked by previous studies.

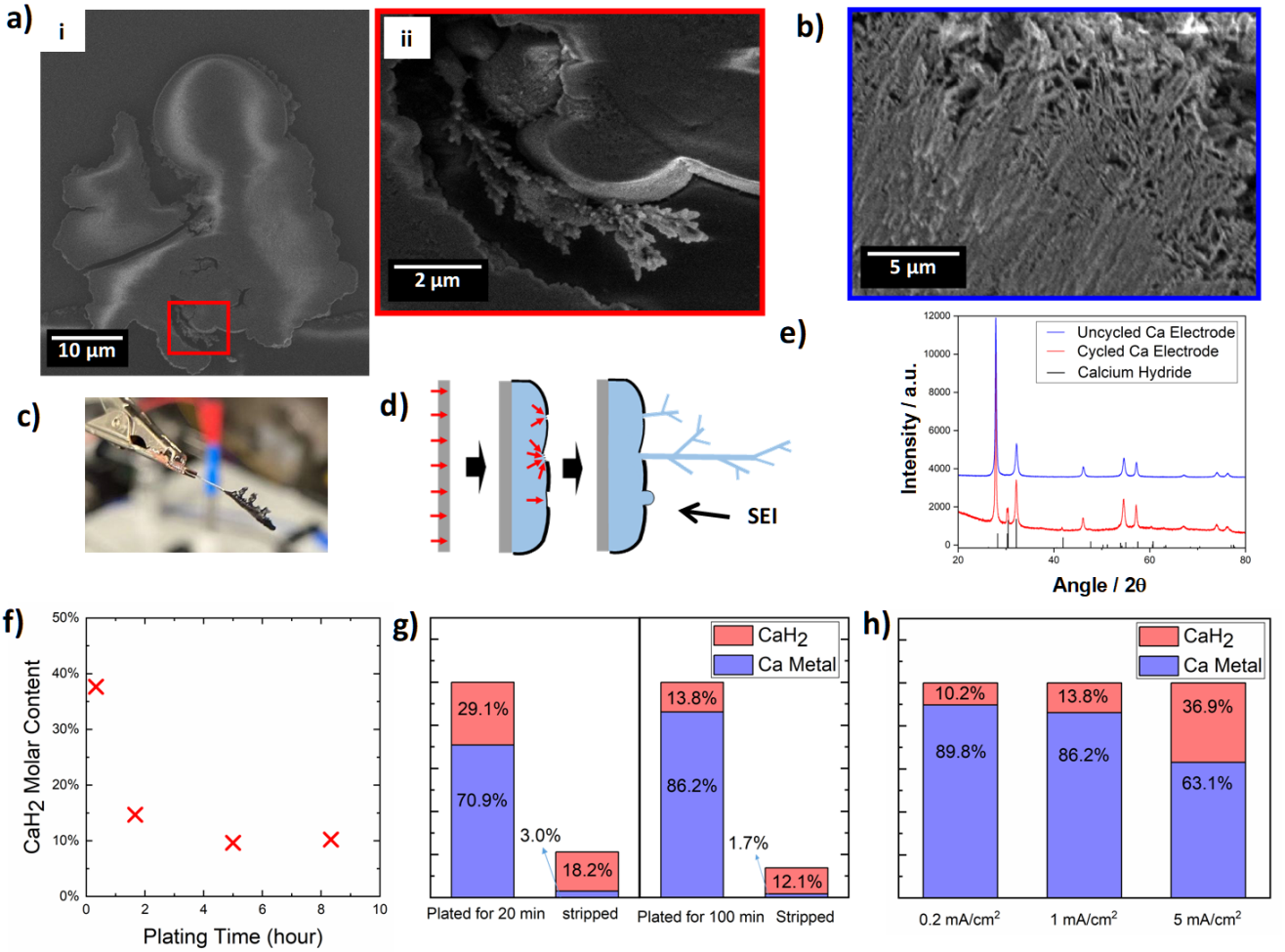

Figure 4. Characterizing the passivating SEI layer. (a) i: SEM image of a Ca globular plating deposit formed

at 10 mA cm^{-2}. ii: Magnified view of the indicated area reveals that a dendrite has formed, potentially due to localized high-current density caused by a heterogeneous SEI layer. (b) SEM cross-section image of potentiostatically plated Ca on a Pt foil working electrode from an electrolytic cell reveals localized dendrites (see also Supporting Figure S7). (c) Post-mortem photograph of dendritic deposition after galvanostatic plating at 5 mA cm^{-2} for 5 hrs. (d) The influence of SEI inhomogeneity on dendrite nucleation (plated Ca blue, SEI layer black, current red). (e) XRD showing the formation of CaH_2 on the metallic Ca plate after cycling for 10 hours. (f)-(h): DEMS measurements for Ca/CaH_2 ratio plated onto Pt foils. (f) The mol% CaH_2 content of the deposit with respect to plating time at constant plating current of 0.2 mA cm^{-2}. (g) Comparison of the Ca/CaH_2 ratio after plating at 1 mA cm^{-2} for 20 min and 100 min, and after stripping. (h) The Ca/CaH_2 ratio after plating at different current densities but with constant total charge; 0.2 mA cm^{-2} for 500 min, 1 mA cm^{-2} for 100 min, 5 mA cm^{-2} for 20 min.

A systematic study of Ca plating morphology was performed with a Ca-ion electrolyte that shows great potential for developing Ca-ion batteries as a next-generation battery system. By using in situ TEM, we show the real-time Ca plating processes with different current density regimes. A transition from globular to dendritic growth was observed as we increased the plating current density, in agreement with the expected behavior of an electroplated metal, and we observed the real-time formation of electrochemically isolated dead Ca deposits during stripping. Dendrite growth was occasionally observed under current density conditions that were well below that expected from the standard electroplating model, which we propose was due to the presence of an irregular SEI layer. The inhomogeneous nature of the SEI led to the presence of localized high current density regions that promoted dendritic deposition. Our work highlights that while Ca-ion batteries hold promise, challenges remain in understanding and managing their chemistry before they can be considered viable.

Acknowledgements

We thank the support and acknowledge use of the facilities of the DCCEM, at the Materials Department, Oxford (EP/R010145/1). JL thanks the support of the 111 project of China (D17003). P.G.B. is indebted to the Engineering and Physical Sciences Research Council (EPSRC), including the SUPERGEN Energy Storage Hub [EP/L019469/1], Enabling Next Generation Lithium Batteries [EP/M009521/1], Henry Royce Institute for Advanced Materials [EP/R00661X/1, EP/S019367/1, EP/R010145/1] and the Faraday Institution All-Solid-State Batteries with Li and Na Anodes [FIRG007, FIRG008] for financial support. AWR thanks the support of the Royal Society.

Supporting Information

Supporting Information is available at DOI:xxx, including electrolyte preparation methods and electrochemical characterization, liquid-cell details, potential plots, additional SEM images, and in-situ TEM movies.

Methods

All preparations and experiments were conducted in argon gloveboxes or sealed systems. A Ca-ion based electrolyte was prepared as 1 M $Ca(BH_4)_2$ dissolved in tetrahydrofuran (THF), as per the work of Wang *et al*.[4] The electrolyte was flown into the encapsulated liquid-cell TEM set-up[32] using a Protochips Poseidon 510 holder, as shown in Figure S1. A thin layer of electrolyte was confined between two Si-SiN chips, with a 120 nm spacer and a flow rate of 80 µl h^{-1} used during TEM imaging. The galvanostatic electrochemical study was performed by applying constant current between the working and counter Pt electrodes patterned on the chip via a Gamry Reference 600. After the TEM imaging experiments, THF was flown into the cell for 2 hours at a rate of 200 µl h^{-1} to wash away all the unreacted Ca electrolyte before the whole cell was taken into a glovebox and disassembled. The disassembled chips were examined using a Carl Zeiss Merlin SEM. Three different current densities

were used for the in-situ TEM study, 1, 10 and 100 mA cm^{-2}. 20 and 50 mA cm^{-2} were also performed within the same set-up but only looked at post-mortem with SEM. The TEM JEOL 3000, operated at 300 kV, was set to use a 50-micron condenser aperture and a spot size 2. Using a Faraday cup the TEM beam current was measured at these conditions, with the dose determined to be ≤ 0.04 electrons $Å^{-2}$ s^{-1} for the condenser lens value used for our TEM imaging experiments. We minimized the total continuous imaging time to no more than 150 s, and then beam blanked between experiments to minimize beam damage and allow electrolyte replenishment.

X-ray diffraction was performed using a Rigaku MiniFlex 600 in a nitrogen environment glovebox.

DEMS was used to quantitatively compare the amount of $Ca:CaH_2$ within the deposit. For every study, galvanostatic plating was performed on a Pt foil as the working electrode and a Ca plate as the counter electrode. After plating, the Pt foil was washed with THF, dried, sealed in a vial then connected to the DEMS. 1 ml of 1M D_2SO_4 in D_2O (dideuterosulfuric acid solution) was added into the vial containing the deposited electrode. The $Ca:CaH_2$ ratio within the deposit can be found from the amount of D_2 and DH gas detected using DEMS, according to the following reaction:[4]

$$Ca+D_2SO_4 \rightarrow D_2 +CaSO_4$$

$$CaH_2 +D_2 \rightarrow 2HD+CaSO_4$$

ToC Graphic

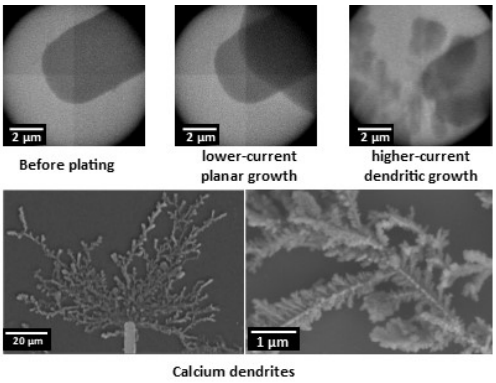

References

(1) Muldoon, J.; Bucur, C. B.; Gregory, T. Quest for Nonaqueous Multivalent Secondary Batteries: Magnesium and Beyond. *Chemical Reviews*. American Chemical Society December 10, 2014, pp 11683–11720. https://doi.org/10.1021/cr500049y.

(2) Yoo, H. D.; Shterenberg, I.; Gofer, Y.; Gershinsky, G.; Pour, N.; Aurbach, D. Mg Rechargeable Batteries: An on-Going Challenge. *Energy and Environmental Science*. August 2013, pp 2265–2279. https://doi.org/10.1039/c3ee40871j.

(3) Lin, M. C.; Gong, M.; Lu, B.; Wu, Y.; Wang, D. Y.; Guan, M.; Angell, M.; Chen, C.; Yang, J.; Hwang, B. J.; et al. An Ultrafast Rechargeable Aluminium-Ion Battery. *Nature* **2015**, *520* (7547), 325–328. https://doi.org/10.1038/nature14340.

(4) Wang, D.; Gao, X.; Chen, Y.; Jin, L.; Kuss, C.; Bruce, P. G. Plating and Stripping Calcium in an Organic Electrolyte. *Nat. Mater.* **2018**, *17* (1), 16–20. https://doi.org/10.1038/NMAT5036.

(5) Son, S. B.; Gao, T.; Harvey, S. P.; Steirer, K. X.; Stokes, A.; Norman, A.; Wang, C.; Cresce, A.; Xu, K.; Ban, C. An Artificial Interphase Enables Reversible Magnesium Chemistry in Carbonate

Electrolytes. *Nat. Chem.* **2018**, *10* (5), 532–539. https://doi.org/10.1038/s41557-018-0019-6.

(6) Aurbach, D.; Cohen, Y.; Moshkovich, M. The Study of Reversible Magnesium Deposition by in Situ Scanning Tunneling Microscopy. *Electrochem. Solid-State Lett.* **2001**, *4* (8). https://doi.org/10.1149/1.1379828.

(7) Matsui, M. Study on Electrochemically Deposited Mg Metal. *J. Power Sources* **2011**, *196* (16), 7048–7055. https://doi.org/10.1016/j.jpowsour.2010.11.141.

(8) Yu, X.; Manthiram, A. Performance Enhancement and Mechanistic Studies of Magnesium-Sulfur Cells with an Advanced Cathode Structure. *ACS Energy Lett.* **2016**, *1* (2), 431–437. https://doi.org/10.1021/acsenergylett.6b00213.

(9) Keyzer, E. N.; Glass, H. F. J.; Liu, Z.; Bayley, P. M.; Dutton, S. E.; Grey, C. P.; Wright, D. S. Mg(PF6)2-Based Electrolyte Systems: Understanding Electrolyte-Electrode Interactions for the Development of Mg-Ion Batteries. *J. Am. Chem. Soc.* **2016**, *138* (28), 8682–8685. https://doi.org/10.1021/jacs.6b04319.

(10) Ta, K.; Zhang, R.; Shin, M.; Rooney, R. T.; Neumann, E. K.; Gewirth, A. A. Understanding Ca Electrodeposition and Speciation Processes in Nonaqueous Electrolytes for Next-Generation Ca-Ion Batteries. *ACS Appl. Mater. Interfaces* **2019**, *11* (24), 21536–21542. https://doi.org/10.1021/acsami.9b04926.

(11) Li, Z.; Fuhr, O.; Fichtner, M.; Zhao-Karger, Z. Towards Stable and Efficient Electrolytes for Room-Temperature Rechargeable Calcium Batteries. *Energy Environ. Sci.* **2019**. https://doi.org/10.1039/c9ee01699f.

(12) Ponrouch, A.; Rosa Palacín, M. Post-Li Batteries: Promises and Challenges. *Philosophical Transactions of the Royal Society A: Mathematical, Physical and Engineering Sciences*. Royal Society Publishing August 26, 2019. https://doi.org/10.1098/rsta.2018.0297.

(13) Canepa, P.; Sai Gautam, G.; Hannah, D. C.; Malik, R.; Liu, M.; Gallagher, K. G.; Persson, K. A.; Ceder, G. Odyssey of Multivalent Cathode Materials: Open Questions and Future Challenges. *Chem. Rev.* **2017**, *117* (5), 4287–4341. https://doi.org/10.1021/acs.chemrev.6b00614.

(14) Staniewicz, R. J. A Study of the Calcium-Thionyl Chloride Electrochemical System. *J. Electrochem. Soc.* **1980**, *127* (4), 782–789. https://doi.org/10.1149/1.2129758.

(15) Meitav, A.; Peled, E. Calcium-Ca(AICI4)2-Thionyl Chloride Cell: Performance and Safety. *J. Electrochem. Soc.* **1982**, *129* (3), 451–457. https://doi.org/10.1149/1.2123879.

(16) Aurbach, D.; Skaletsky, R.; Gofer, Y. The Electrochemical Behavior of Calcium Electrodes in a Few Organic Electrolytes. *J. Electrochem. Soc.* **1991**, *138* (12), 3536–3545. https://doi.org/10.1149/1.2085455.

(17) Ponrouch, A.; Frontera, C.; Bardé, F.; Palacín, M. R. Towards a Calcium-Based Rechargeable Battery. *Nat. Mater.* **2016**, *15* (2), 169–172. https://doi.org/10.1038/nmat4462.

(18) Arroyo-De Dompablo, M. E.; Ponrouch, A.; Johansson, P.; Palacín, M. R. Achievements, Challenges, and Prospects of Calcium Batteries. *Chemical Reviews*. American Chemical Society 2019. https://doi.org/10.1021/acs.chemrev.9b00339.

(19) Shakourian-Fard, M.; Kamath, G.; Taimoory, S. M.; Trant, J. F. Calcium-Ion Batteries: Identifying Ideal Electrolytes for Next-Generation Energy Storage Using Computational

Analysis. *J. Phys. Chem. C* **2019**, *123* (26), 15885–15896. https://doi.org/10.1021/acs.jpcc.9b01655.

(20) Ponrouch, A.; Palacin, M. R. On the Road toward Calcium-Based Batteries. *Current Opinion in Electrochemistry*. Elsevier B.V. June 1, 2018, pp 1–7. https://doi.org/10.1016/j.coelec.2018.02.001.

(21) Gummow, R. J.; Vamvounis, G.; Kannan, M. B.; He, Y. Calcium-Ion Batteries: Current State-of-the-Art and Future Perspectives. *Advanced Materials*. September 2018, p 1801702. https://doi.org/10.1002/adma.201801702.

(22) Shyamsunder, A.; Blanc, L. E.; Assoud, A.; Nazar, L. F. Reversible Calcium Plating and Stripping at Room Temperature Using a Borate Salt. *ACS Energy Lett.* **2019**, *4* (9), 2271–2276. https://doi.org/10.1021/acsenergylett.9b01550.

(23) Davidson, R.; Verma, A.; Santos, D.; Hao, F.; Fincher, C.; Xiang, S.; Van Buskirk, J.; Xie, K.; Pharr, M.; Mukherjee, P. P.; et al. Formation of Magnesium Dendrites during Electrodeposition. *ACS Energy Lett.* **2019**, *4* (2), 375–376. https://doi.org/10.1021/acsenergylett.8b02470.

(24) Mehdi, B. L.; Qian, J.; Nasybulin, E.; Park, C.; Welch, D. A.; Faller, R.; Mehta, H.; Henderson, W. A.; Xu, W.; Wang, C. M.; et al. Observation and Quantification of Nanoscale Processes in Lithium Batteries by Operando Electrochemical (S)TEM. *Nano Lett.* **2015**, *15* (3), 2168–2173. https://doi.org/10.1021/acs.nanolett.5b00175.

(25) Sacci, R. L.; Dudney, N. J.; More, K. L.; Parent, L. R.; Arslan, I.; Browning, N. D.; Unocic, R. R. Direct Visualization of Initial SEI Morphology and Growth Kinetics during Lithium Deposition by in Situ Electrochemical Transmission Electron Microscopy. *Chem. Commun.* **2014**, *50* (17),

2104–2107. https://doi.org/10.1039/c3cc49029g.

(26) Fang, C.; Li, J.; Zhang, M.; Zhang, Y.; Yang, F.; Lee, J. Z.; Lee, M. H.; Alvarado, J.; Schroeder, M. A.; Yang, Y.; et al. Quantifying Inactive Lithium in Lithium Metal Batteries. *Nature*. Nature Publishing Group August 22, 2019, pp 511–515. https://doi.org/10.1038/s41586-019-1481-z.

(27) White, E. R.; Singer, S. B.; Augustyn, V.; Hubbard, W. A.; Mecklenburg, M.; Dunn, B.; Regan, B. C. In Situ Transmission Electron Microscopy of Lead Dendrites and Lead Ions in Aqueous Solution. *ACS Nano* **2012**, *6* (7), 6308–6317. https://doi.org/10.1021/nn3017469.

(28) Schneider, N. M.; Park, J. H.; Grogan, J. M.; Steingart, D. A.; Bau, H. H.; Ross, F. M. Nanoscale Evolution of Interface Morphology during Electrodeposition. *Nat. Commun.* **2017**, *8* (1), 2174. https://doi.org/10.1038/s41467-017-02364-9.

(29) Kraus, T.; De Jonge, N. Dendritic Gold Nanowire Growth Observed in Liquid with Transmission Electron Microscopy. *Langmuir* **2013**, *29* (26), 8427–8432. https://doi.org/10.1021/la401584z.

(30) Bai, P.; Li, J.; Brushett, F. R.; Bazant, M. Z. Transition of Lithium Growth Mechanisms in Liquid Electrolytes. *Energy Environ. Sci.* **2016**, *9* (10), 3221–3229. https://doi.org/10.1039/c6ee01674j.

(31) Song, B.; Dhiman, I.; Carothers, J. C.; Veith, G. M.; Liu, J.; Bilheux, H. Z.; Huq, A. Dynamic Lithium Distribution upon Dendrite Growth and Shorting Revealed by Operando Neutron Imaging. *ACS Energy Lett.* **2019**, *4* (10), 2402–2408. https://doi.org/10.1021/acsenergylett.9b01652.

(32) Pu, S.; Gong, C.; Robertson, A. W. Liquid Cell Transmission Electron Microscopy and Its Applications. *R. Soc. Open Sci.* **2020**, *7* (1), 191204. https://doi.org/10.1098/rsos.191204.

(33) Williamson, M. J.; Tromp, R. M.; Vereecken, P. M.; Hull, R.; Ross, F. M. Dynamic Microscopy of Nanoscale Cluster Growth at the Solid–Liquid Interface. *Nat. Mater.* **2003**, *2* (8), 532–536. https://doi.org/10.1038/nmat944.

(34) Radisic, A.; Ross, F. M.; Searson, P. C. In Situ Study of the Growth Kinetics of Individual Island Electrodeposition of Copper. *J. Phys. Chem. B* **2006**, *110* (15), 7862–7868. https://doi.org/10.1021/jp057549a.

(35) Ross, F. M. Opportunities and Challenges in Liquid Cell Electron Microscopy. *Science (80-.).* **2015**, *350* (6267), 1490. https://doi.org/10.1126/science.aaa9886.

(36) Sa, N.; Rajput, N. N.; Wang, H.; Key, B.; Ferrandon, M.; Srinivasan, V.; Persson, K. A.; Burrell, A. K.; Vaughey, J. T. Concentration Dependent Electrochemical Properties and Structural Analysis of a Simple Magnesium Electrolyte: Magnesium Bis(Trifluoromethane Sulfonyl)Imide in Diglyme. *RSC Adv.* **2016**, *6* (114), 113663–113670. https://doi.org/10.1039/c6ra22816j.